HHS Public Access

Author manuscript

Nat Cell Biol. Author manuscript; available in PMC 2013 May 01.

Published in final edited form as:

Nat Cell Biol. 2012 November ; 14(11): 1192–1202. doi:10.1038/ncb2595.

Canonical and Atypical E2Fs Regulate the Mammalian Endocycle

Hui-Zi Chen[1,2,*], **Madhu M. Ouseph**[1,3,*], **Jing Li**[1,§], **Thierry Pécot**[1,4,5], **Veda Chokshi**[1], **Lindsey Kent**[1], **Sooin Bae**[1], **Morgan Byrne**[1], **Camille Duran**[1], **Grant Comstock**[1], **Prashant Trikha**[1], **Markus Mair**[1], **Shantibhusan Senapati**[1], **Chelsea K. Martin**[1], **Sagar Gandhi**[1], **Nicholas Wilson**[1], **Bin Liu**[1,5], **Yi-Wen Huang**[7], **John C. Thompson**[1], **Sundaresan Raman**[4], **Shantanu Singh**[4], **Marcelo Leone**[4], **Raghu Machiraju**[4], **Kun Huang**[5], **Xiaokui Mo**[6], **Soledad Fernandez**[6], **Ilona Kalaszczynska**[9], **Debra J. Wolgemuth**[8], **Piotr Sicinski**[9], **Tim Huang**[1], **Victor Jin**[5], and **Gustavo Leone**[1,2,ζ]

[1]Solid Tumor Biology Program, Department of Molecular Virology, Immunology and Medical Genetics, Comprehensive Cancer Center; The Ohio State University, Columbus, Ohio 43210, USA

[2]Medical Scientist Training Program and Integrated Biomedical Graduate Program, College of Medicine; The Ohio State University, Columbus, Ohio 43210, USA

[3]Ohio State Biochemistry Program, The Ohio State University, Columbus, Ohio 43210, USA

[4]Computer Science and Engineering, The Ohio State University, Columbus, Ohio 43210, USA

[5]Biomedical Informatics, The Ohio State University, Columbus, Ohio 43210, USA

[6]Center for Biostatistics, Office of Health Sciences, The Ohio State University, Columbus, Ohio 43210, USA

[7]Department of Obstetrics and Gynecology, Medical College of Wisconsin, Milwaukee, Wisconsin 53226, USA

[8]Department of Genetics and Development, Department of Obstetrics and Gynecology, The Institute of Human Nutrition, and The Herbert Irving Comprehensive Cancer Center, Columbia University Medical Center, New York, New York 10032, USA

[ζ]Corresponding Author Information: Gustavo Leone, Ph.D., Solid Tumor Biology Program, Department of Molecular Virology, Immunology and Medical Genetics, Department of Molecular Genetics, The Ohio State University, Comprehensive Cancer Center, 460 W. 12th Ave., Room 592, Columbus, OH 43210, Telephone: 614-688-4567, Fax: 614-292-3312, Gustavo.Leone@osumc.edu.

[*]Authors contributed equally to this work

[§]Current address: Roche Molecular Systems, 4300 Hacienda Drive, Pleasanton, CA 94588

AUTHOR CONTRIBUTIONS

H.-Z.C., M.M.O., J.L., and G.L. designed the experiments. H.-Z.C., M.M.O., J.L., T.P., V.C., L.K. and S.B. performed experiments. H.-Z.C. and M.M.O. co-wrote the paper with G.L.; all other authors listed helped perform experiments. Specifically, J.C.T., S.R., S.S., M.L., R.M. and K.H. helped with experiments relating to confocal microscopy and 3D reconstruction. X.M. and S.F. helped analyze data and performed statistics. I.K., D.J.W. and P.S. provided mice for the study and reviewed drafts of the manuscript. T.H., B.L. and V.J. contributed to discussion relating to Affymetrix/NanoString analyses.

The authors declare no competing financial interests

[9]Department of Cancer Biology, Dana-Farber Cancer Institute, and Department of Genetics, Harvard Medical School, Boston, Massachusetts 02215, USA

SUMMARY

The endocycle is a variant cell cycle consisting of successive DNA synthesis and Gap phases that yield highly polyploid cells. Although essential for metazoan development, relatively little is known about its control or physiologic role in mammals. Using novel lineage-specific *cre* mice we identified two opposing arms of the E2F program, one driven by canonical transcription activation (E2F1, E2F2 and E2F3) and the other by atypical repression (E2F7 and E2F8), that converge on the regulation of endocycles *in vivo*. Ablation of canonical activators in the two endocycling tissues of mammals, trophoblast giant cells in the placenta and hepatocytes in the liver, augmented genome ploidy, whereas ablation of atypical repressors diminished ploidy. These two antagonistic arms coordinate the expression of a unique G_2/M transcriptional program that is critical for mitosis, karyokinesis and cytokinesis. These results provide *in vivo* evidence for a direct role of E2F family members in regulating non-traditional cell cycles in mammals.

The archetypal cell division cycle culminates in the generation of genetically identical diploid progenies. However, a number of cell cycle variations in nature exist, with the endocycle being a remarkable variant utilized by a wide range of organisms in diverse environmental contexts[1]. This modified cell cycle is characterized by alternating DNA synthesis (S) and Gap (G) phases in the absence of intervening mitosis (M), karyokinesis and cytokinesis. As a result of successive rounds of whole genome duplication, cells may achieve genome polyploidy that exceed 1000C[2,3]. The biological advantages of polyploidy have been proposed to include an augmented response to strenuous cellular metabolic demands; dampened sensitivity to apoptotic or checkpoint stimuli[4]; and buffering against deleterious mutations that may cause cancer[5,6].

The molecular mechanisms that control mitotic and variant cell cycles among species are presumed to be similar. In the textbook view of cell cycle control, E2F transcriptional activators and repressors are portrayed to orchestrate a gene expression program essential for mitotic cell cycle progression[7], with E2F activators and repressors oppositely regulating a common set of target genes. However, careful analyses of mouse knockout tissues demonstrate that E2F function *in vivo* do not strictly adhere to this elegant dichotomous paradigm[8–16]. This is perhaps not surprising given the large number of genes in the mammalian E2F family, which consists of eight distinct genes encoding at least nine structurally related protein products that can be divided into activator or repressor subclasses[17]. Canonical E2F activators (E2F1, E2F2, E2F3a and E2F3b) have a single DNA binding domain (DBD), heterodimerize with DP1/DP2 proteins and associate with co-activator proteins to robustly induce RNA polymerase II-dependent gene expression[18]. Canonical repressors (E2F4, E2F5 and E2F6) also have a single DBD, heterodimerize with DP1/DP2 proteins and associate with chromatin modifying proteins to repress gene expression[18]. The most recently identified family members encode the atypical repressors E2F7 and E2F8, which have two tandem DBDs and repress gene expression independent of DP1/DP2 heterodimerization[19].

While flies and plants use endocycles as a mechanism for cell growth in a variety of tissue types[1,20], endocycles in mammals are mainly restricted to trophoblast giant cells (TGCs) in the placenta and hepatocytes in the liver[1,5]. Endocycles in these mammalian tissues are believed to be integral to organ physiology[1,5], however, surprisingly little evidence exists to support this contention. Here we developed novel genetic tools in mice and show by depletion of either canonical E2F activators or atypical E2F repressors that these two separate E2F transcriptional programs converge to control the endocycle through the regulation of cellular events important for mitosis, karyokinesis and cytokinesis. Surprisingly, placentas and livers with severely restricted polyploidization retained sufficient physiological function to carry them through apparently normal development.

RESULTS

E2f1-3 Ablation Results in Hyperploidy

E2F mediated transcription contributes to endocycle control in flies and plants[1,5,19–21], but its role in mammals has not been thoroughly evaluated. Whole genome duplication in mammalian endocycling cells is temporally regulated during development with major ploidy increases in TGCs during mid gestation and in hepatocytes following weaning at around three weeks of age[22,23]. The levels of *E2f1* and *E2f2* mRNAs in laser capture microdissected TGCs from wildtype placentas, as measured by NanoString technology (Fig. 1a), were low throughout placental development, whereas the level of *E2f3* mRNA was high prior to E8.5 and following E13.5. Expression analysis in livers by quantitative real-time polymerase chain reaction (qRT-PCR) showed relatively high levels of *E2f1* and *E2f2* during fetal development and a precipitous decrease following birth (P0), whereas expression of *E2f3* (*E2f3a* and *E2f3b*) decreased gradually following birth and was almost undetectable post-weaning (Fig. 1b). Consistent with the expression pattern of their mRNAs, E2F3a and E2F3b protein levels decreased in newborn pups post weaning (Supplementary Fig. 1a), while E2F1 and E2F2 proteins could not be detected beyond the intrauterine period (data not shown). Thus, it would appear that total E2F1-3 activator levels are minimized when TGCs and hepatocytes are most actively endocycling.

We utilized targeted gene inactivation strategies in mice to rigorously evaluate the role of E2F activators in endocycling TGCs and hepatocytes. To avoid functional compensation[24], we evaluated TGCs in embryos deficient for the entire E2F activator subclass (*E2f1-3*). Visual inspection of H&E stained E9.5 *E2f1*$^{-/-}$;*E2f2*$^{-/-}$;*E2f3*$^{-/-}$ (*123tko*) placentas revealed the presence of TGCs with abnormally large nuclei (Fig. 1c). Feulgen staining and quantification of genome ploidy by standardized methods (Supplementary Fig. 1b) showed a further shift of the *123tko* TGC population towards higher ploidy (Fig. 1d and Supplementary Fig. 1c). Analysis of *123tko* TGCs at later stages of development was precluded due to embryo lethality at E10.5[25,26].

To evaluate the role of the three activator E2Fs in hepatocytes we used pIpC-inducible *Mx-cre* mice[27] and conditional alleles of *E2f3* (*Mx-cre;E2f1*$^{-/-}$;*E2f2*$^{-/-}$;*E2f3*$^{f/f}$; *Mx-123tko*) to examine the consequences of their combined ablation. Injection of pIpC in six-week-old *Mx-123tko* mice resulted in increased liver weights (Fig. 1f) and proportionately larger hepatocytes (Fig. 1e, f) than age-matched controls. Loss of *E2f1* alone or in combination

with *E2f2* and *E2f3* resulted in a gene dose-dependent increase in hepatocyte ploidy (Fig. 1g and Supplementary Fig. 1d). The expression of *E2f* repressors (*E2f4-8*) was not affected by loss of *E2f1-3* (Supplementary Fig. 1e). Together, these findings suggest that mammalian E2F activators have a physiologic role in suppressing endocycles.

E2f7/E2f8 Ablation Reduces TGC Ploidy

Next, we explored the role of E2F repressors in endocycle control. Expression analysis of the canonical repressors (*E2f4-6*) showed relatively high levels of *E2f4* in TGCs of E6.5 placentas that decreased with time, whereas *E2f5-6* expression was relatively constant throughout placental development (Fig. 2a, left panel); expression of *E2f4-6* was relatively high in fetal livers and their expression decreased after birth (Supplementary Fig. 2a). Inspection of $E2f4^{-/-}$ or $E2f5^{-/-}$ embryos and mice revealed normal placentas and livers (Supplementary Fig. 2b, c); $E2f6^{-/-}$ placentas and livers were not evaluated.

We then focused our attention on the atypical repressors, E2F7 and E2F8. These E2Fs are expressed in TGCs throughout placental development (Fig. 2a, right panel). Immunohistochemistry (IHC) showed robust staining of E2F7 and E2F8 proteins in a portion of TGCs (Fig. 2b, arrows), consistent with their established cell cycle dependent expression in late S and G_2 phases[28–31]. Visual inspection of $E2f7^{-/-};E2f8^{-/-}$ placentas at E10.5, one day prior to their embryonic lethality[16], revealed a surprising number of TGCs at various stages of mitosis (Fig. 2c), implying an interruption of normal endocycles. Indeed, the ploidy of $E2f7^{-/-};E2f8^{-/-}$ TGCs never exceeded 64C (Fig. 2d, black bars), whereas wildtype TGCs with genomes >1000C were readily detected (Fig. 2d, white bars). The combined inactivation of *E2f7* and *E2f8* led to ectopic BrdU incorporation (Fig. 2e and 2g), increased levels of G_2/M (cyclin A2) and M phase-specific proteins (cyclin B1 and phosphorylated-H3, P-H3) (Fig. 2f, g) and the appearance of numerous TGCs in metaphase and anaphase (Fig. 2h). Confocal microscopy and 3D reconstruction of serially imaged $E2f7^{-/-};E2f8^{-/-}$ placentas showed that approximately 40% of TGCs contained at least two nuclei (Fig. 2i), which was confirmed by transmission electron microscopy (Fig. 2j). Placentas lacking *E2f7*, *E2f8*, or one allele of each ($E2f7^{+/-};E2f8^{+/-}$) exhibited TGCs with an intermediate reduction in ploidy (Fig. 2d and Supplementary Fig. 2d, e) and a proportionate increase in G_2/M and M phase related events (Fig. 2g and 2j), once again suggesting a gene dosage effect.

Because expression of trophoblast cell lineage markers was altered in placentas globally deleted for *E2f7* and *E2f8* (TGCs, labyrinth trophoblasts and spongiotrophoblasts)[32], we could not formally rule out a general disruption of differentiation as a possible cause for the endocycle defects observed in mutant TGCs. To specifically ablate *E2f7* and *E2f8* in TGCs of placentas we crossed $Plf^{cre/+}$ knockin mice (Fig. 2k and data not shown)[32] with $E2f7^{f/f};E2f8^{f/f}$ mice to yield *Plf-78dko* embryos. We confirmed the TGC-specific ablation of conditional alleles by PCR genotyping of laser capture microdissected samples (Fig. 2l). The same abnormalities were observed in *Plf-78dko* TGCs as in $E2f7^{-/-};E2f8^{-/-}$ TGCs, including the reduced ploidy, increased cyclin A2, cyclin B1 and P-H3 expression levels, and ectopic karyokinesis (Fig. 2d, 2g and 2j; red bars). In summary, these data demonstrate

cell autonomous functions for E2F7 and E2F8 in facilitating TGC endocycles by repressing key molecular events required for mitosis and karyokinesis.

E2f7/E2f8 Ablation Prevents Hepatocyte Endocycles

The expression of *E2f7* and *E2f8* in fetal livers was high but decreased to almost undetectable levels by weaning age (Fig. 3b and Supplementary Fig. 3a). To examine their roles during postnatal liver development we crossed $E2f7^{f/f}$ and $E2f8^{f/f}$ mice with *Albumin-cre* mice (*Alb-cre*)[33], which express *cre* in hepatocytes of late term embryos and newborn pups. The conditional inactivation of *E2f7* (*Alb-7ko*), *E2f8* (*Alb-7ko*) or both (*Alb-78dko*) did not significantly affect hepatic mass (Supplementary Fig. 3b). However, evaluation of H&E and DAPI stained liver sections from *Alb-8ko* and *Alb-78dko* mice revealed markedly smaller hepatocytes with smaller nuclei than in control animals (Fig. 3a and 3c). This reduction in cell size was compensated by an increase in the total number of hepatocytes (Fig. 3d). Moreover, *Alb-8ko* and *Alb-78dko* livers had a decreased proportion of binucleated hepatocytes (Fig. 3e), which is an early event believed to precede the onset of polyploidization[34]. Strikingly, flow cytometry showed that hepatocytes in *Alb-8ko* and *Alb-78dko* livers remained diploid over the entire lifetime of the mouse, whereas hepatocytes in *Alb-7ko* livers had only a modest reduction in genome ploidy (Fig. 3f). The percentages of Ki67-, cyclin A2-, cyclin B1- and P-H3-positive hepatocytes were significantly elevated in 2-month-old *Alb-8ko* mice and even more so in similarly aged *Alb-78dko* mice (Fig. 3g). Analysis of mice globally deleted for *E2f7* ($E2f7^{-/-}$) or *E2f8* ($E2f8^{-/-}$) yielded identical phenotypes as conditionally deleted *Alb-7ko* and *Alb-8ko* mice (Supplementary Fig. 3c, d). Surprisingly, *Alb-78dko* mice survived to old age in apparent good health and retained the capacity to regenerate their livers upon chemical (carbon tetrachloride) or physical (partial hepatectomy) injury (Supplementary Fig. 3e-h and data not shown). From these results, we conclude that E2F8 is the principal atypical E2F that functions to promote hepatocyte endocycles in mice.

The onset of genome endoreduplication in hepatocytes coincides with the weaning of pups, but DNA content continues to increase through adulthood even though very little *E2f8* is expressed at this time (see Fig. 3b). These observations raised the possibility that E2F8 might only be required for the programmed onset and not the continuation of endocycles. We thus used a tamoxifen-inducible system (*SA-creER*^{T2}) to express *cre* in hepatocytes following birth and/or the weaning of pups[35]. As determined by qRT-PCR, supplying *SA-creER*^{T2}*;E2f8*$^{f/f}$ mice with a tamoxifen diet beginning at either 7 days (two weeks before weaning, pre-weaning) or 28 days of age (one week following weaning, post-weaning) resulted in the tissue-specific efficient deletion of *E2f8* (data not shown). Ablation of *E2f8* pre-weaning prevented efficient polyploidization of hepatocytes (Supplementary Fig. 4a-c), whereas ablation post-weaning failed to impact hepatocyte size, binucleation and DNA content (data not shown and Supplementary Fig. 4a, 4b and 4d). These results suggest that E2F8 is largely dispensable for the execution of endocycles following the weaning of pups.

E2F7/E2F8 Regulate Endocycle-related Genes

Given the role of E2F7 and E2F8 in transcriptional repression, we anticipated changes in gene expression as the principal underlying cause for the observed endocycle defects in

E2f7/E2f8 deficient tissues. Gene expression profiling (Affymetrix Mouse Genome 430 2.0) using RNA purified from livers of 3-week-old wildtype, *Alb-7ko*, *Alb-8ko* and *Alb-78dko* mice showed that there were significantly more upregulated than downregulated genes in mutant tissues, consistent with their roles as repressors (Fig. 4a). Expression changes were confirmed by NanoString technology (Supplementary Fig. 5a). Supervised clustering methods identified three main classes of differentially expressed genes (Fig. 4a). Class I includes genes differentially expressed in all three mutant genetic groups relative to wildtype controls. These genes may represent targets regulated by both E2F7 and E2F8 since loss of either member led to their derepression. Class II represent genes differentially expressed in two of the three mutant genetic groups and include target genes that may be uniquely repressed by either E2F7 or E2F8. Finally, class III represent genes differentially expressed in only one mutant genetic group, and include target genes that may be synergistically repressed by E2F7 and E2F8.

Further analysis focused on genes upregulated in both *Alb-8ko* and *Alb-78dko* livers (Class II), since hepatocytes in these two genetic groups displayed the most pronounced reduction in genome ploidy, as well as genes upregulated in all three mutant cohorts (in Class I), since these could also contribute to the observed defect in polyploidization. Closer inspection of these genes by Ingenuity Pathway Analysis (IPA) revealed a striking bias for functions related to cytokinesis, G_2/M progression and various stages of mitosis, such as chromosome condensation, stabilization and segregation (Supplementary Fig. 5b, c). By manual annotation we also noted an increase in gene products with GTPase-activating (GAP) or GTP exchange factor (GEF) functions (data not shown), which regulate Rho family of small GTPases essential for successful cytokinesis[36]. NanoString technology was then used to interrogate the expression of a panel of genes with cell cycle and G_2/M related functions in TGCs from E10.5 wildtype, *E2f7*$^{-/-}$, *E2f8*$^{-/-}$ and *E2f7*$^{-/-}$;*E2f8*$^{-/-}$ placentas. As shown in Figure 4b, 66 of the 99 genes interrogated had predominantly increased expression in *E2f7/E2f8* deficient TGCs, suggesting a common mechanism for how E2F7 and E2F8 may regulate endocycles in TGCs and hepatocytes.

A significant portion of common upregulated genes in *E2f7/E2f8* deficient TGCs and hepatocytes have E2F binding elements on their promoters, raising the possibility that these may represent direct targets of E2F7/E2F8. To test this hypothesis, we transfected human HepG2 cells and rat Rcho-1 trophoblast stem (TS) cells with plasmids expressing Flag-tagged E2F7 (F7) or E2F8 (F8) and performed chromatin immunoprecipitation (ChIP) assays with anti-Flag antibodies. As shown in Figures 5b and 5d, Flag-specific antibodies, but not control IgG, co-immunoprecipitated promoter sequences containing E2F binding elements, but not irrelevant sequences lacking E2F binding sites (*Tub*). The above results were corroborated by additional ChIP assays in human embryonic kidney (HEK) 293 cells transfected with either F7 or F8 (Supplementary Fig. 5d) and in wildtype liver tissues transfected by hydrodynamic-based methods with plasmids expressing F8 (Fig. 5e, f). Together, these results suggest that E2F7 and E2F8 repress a core group of genes with prominent involvement in the regulation of G_2/M related events.

E2F1 Functionally Opposes Atypical E2F7/E2F8

Given that ablation of *E2f1-3* and *E2f7/E2f8* led to opposite effects on hepatocyte ploidy, we explored the possibility of cross-regulation between these two E2F subclasses. Loss of *E2f1-3* did not impact the expression of other E2Fs (*E2f4-8*; see Supplementary Fig. 1e), however, loss of *E2f7/E2f8* resulted in a transient increase of *E2f1* expression soon after birth in the liver (Supplementary Fig. 5e). Interestingly, loss of *E2f7/E2f8* had no significant effect on the expression of *E2f1-6* in TGCs (Supplementary Fig. 5f). We then profiled global gene expression in hepatocytes lacking the three E2F activators (*Mx-123tko*). Strikingly, this analysis showed that the majority of genes upregulated in *E2f7/E2f8* deficient hepatocytes were downregulated in *E2f1-3* deficient hepatocytes (Fig. 4c), and many of these genes had annotated 'cell cycle' functions related to G_2/M transitions or mitoses and had E2F binding sites in their promoters (Fig. 4d and Supplementary Fig. 5g, h).

Based on the above results we entertained the hypothesis that canonical E2F activators may functionally antagonize atypical E2F repressors in the control of endocycles. To rigorously test this possibility we generated and analyzed mice with TGCs or hepatocytes deficient for E2F7, E2F8 and E2F1 ($E2f1^{-/-}$). The ablation of $E2f7^{f/f}$ and $E2f8^{f/f}$ alleles in TGCs was achieved by $Plf^{cre/+}$ (*Plf-178tko*) and their ablation in hepatocytes was achieved by *Alb-cre* (*Alb-178tko*). Placenta sections from E10.5 *Plf-178tko* embryos exhibited TGCs with large nuclei having increased ploidy (Fig. 6a), with some TGCs having 128C and 256C genomes (Fig. 6b), which was never observed in *Plf-78dko* TGCs. This increase in ploidy was accompanied by a significant decrease in the number of multinucleated TGCs and a slight decrease in BrdU- and P-H3-positive cells, even though the number of cyclin A2-positive TGCs was not reduced (Fig. 6c). Similar results were obtained when placentas globally deleted for *E2f1*, *E2f7* and *E2f8* (*178tko*) were examined (Supplementary Fig. 6a-c). Evaluation of *Alb-178tko* livers revealed larger hepatocytes containing greater DNA content than in *Alb-78dko* livers, with some reaching 8C ploidy (Fig. 6d-f). The *Alb-178tko* livers also had many more binucleated hepatocytes (Fig. 6g), and importantly, had fewer Ki67-, P-H3- and cyclin B1-positive hepatocytes, even though again, the percentage of cyclin A2-positive cells was not reduced (Fig. 6h). Thus it would appear that loss of *E2f1* suppressed some but not all mitotic defects in TGCs and hepatocytes caused by *E2f7/E2f8* deficiency.

Loss of Cyclin A2 Reinstates G_2/M Block and Polyploidy in *E2f7/E2f8* Deficient Cells

Because the inactivation of *E2f7/E2f8* results in ectopic mitoses without inhibiting DNA replication, we predicted that re-establishing a mitotic block would restore polyploidy in *E2f7/E2f8* deficient cells. Previous analysis of TS cell cultures showed that $p57^{KIP2}$ activity participates in driving TGC differentiation and endocycles by inhibiting Cdk1 function[37]. However, we failed to detect any measureable change in $p57^{KIP2}$ mRNA or protein levels that might underlie the phenotype of *E2f7/E2f8* deficient TGCs or hepatocytes (Supplementary Fig. 6d). Given that cyclin A activity is critical for G_2/M progression by regulating the APC/Cyclosome[38], we sought to evaluate the consequence of inactivating cyclin A1/A2 in *E2f7/E2f8* deficient TGCs and hepatocytes. We thus intercrossed $Ccna1^{-/-};Ccna2^{f/f}$ mice[39] with $Plf^{cre/+};E2f7^{f/f};E2f8^{f/f}$ and generated embryos with quadruply deficient TGCs (*Plf-*A^{12}*78qko*). Remarkably, TGCs in E10.5 *Plf-*A^{12}*78qko* embryos had larger nuclei with greater DNA content than TGCs in *Plf-78dko* embryos, with

some reaching 1024C (Fig. 7a, b). We also intercrossed *Ccna1*$^{-/-}$;*Ccna2*$^{f/f}$ mice with *Alb-cre;E2f7*$^{f/f}$;*E2f8*$^{f/f}$ mice to generate offspring with quadruply deficient hepatocytes (*Alb-A*^{12}*78qko*). As shown in Figure 7d, hepatocytes in 3-month-old *Alb-A*^{12}*78qko* mice had similar ploidy levels as in age-matched wildtype mice. Interestingly, the loss of *Ccna1/Ccna2* alone (*Alb-A*^{12}*dko*) in hepatocytes resulted in hyperploidy (Fig. 7c, d). In summary, inhibiting the transcriptional network that signals G_2/M progression (by *E2f1* inactivation) or interfering with the mitotic machinery (by *Ccna1/Ccna2* inactivation) re-established a mitotic block and reinstated higher levels of polyploidy in *E2f7/E2f8* deficient cells.

DISCUSSION

In multi-cellular organisms there exists diversity in the kinetics and composition of cell cycles and presumably, in the mechanisms that regulate them. The endocycle is commonly utilized in flies and plants and hence, more is known about how they are controlled in these organisms than in mammals[40–45]. The balanced action of the E2F activator (*dE2f1*) and repressor (*dE2f2*) in *Drosophila* is critical for the tight regulation of cyclin E expression and successful completion of S phase in mitotic and endocycling cells[21,42,43]. While E2Fs are also involved in controlling endocycles in plants, their role appears to be different than in mammals. For example the atypical E2Fe repressor in *Arabidopsis* is required to prevent endocycles[44], while we show that the atypical E2F7 and E2F8 family members in mice promote endocycles. A comparison of the regulation of how atypical E2Fs are expressed during development and identification of their direct targets might shed light on these differences. In summary, our current work exposes an intricate E2F network involving balanced and antagonistic activities of canonical E2F activators (E2F1-3) and atypical E2F repressors (E2F7-8) that controls mammalian endocycles. Perhaps the most dramatic manifestation of altering the balance in the E2F network is the ectopic mitosis and karyokinesis observed in *E2f7/E2f8* deficient TGCs.

The results presented here expose two distinct arms of the E2F network, one arm involving canonical activators (E2F1-3) and a second involving atypical repressors (E2F7/E2F8), that converge to antagonistically regulate a common gene expression program critical for mammalian endocycles *in vivo*. A similar antagonistic role for E2F activators and atypical repressors appears to be at play in the control of a distinct program that is critical for mitotic cell cycles during placental development[32]. Because neither loss of *E2f4* or *E2f5* in mice[12–14] appeared to affect polyploidization of TGCs and hepatocytes (Supplementary Fig. 2c and data not shown) we propose that the most ancient E2F repressor arm consisting of atypical *E2f7* and *E2f8* evolved to specifically regulate variant cell cycles in metazoans in a manner distinct from the function of canonical E2F repressor proteins. One reason for this might be to keep E2F7/E2F8 mediated repression outside the influence of the cyclin-CDK axis. Because E2F7/E2F8 DNA binding activity is independent of DP proteins, atypical repressors would remain unresponsive to CDK-mediated phosphorylation of DP, which negatively regulates the DNA binding and functions of canonical repressors[45–47], allowing repression at a time (S/G_2) when CDK activity is high. However, the exact molecular mechanism of how canonical activators and atypical repressors coordinate gene expression in endocycling tissues remains obscure.

It has been assumed that polyploidy in mammals, as in flies and plants, is integral to the physiologic functions of placentas and livers. Here we generated the first mouse models with significantly reduced TGC and hepatocyte ploidy to assess this hypothesis. Surprisingly, TGCs and hepatocytes having significantly restricted ploidy levels appeared to impart placentas and livers, respectively, with adequate organ function to carry animals through embryonic and adult development. Whether altered liver ploidy in mice impacts aging-related processes such as tumor development remains to be evaluated. In summary, genetic, systems-based and biochemical approaches revealed a fundamental role for the canonical activator and atypical repressor arms of the E2F network in orchestrating mammalian endocycles *in vivo*.

METHODS

Mouse husbandry and genotyping

All mice were housed in barrier conditions with a 12-hour light/dark cycle and had access to food/water *ad libitum*. Genotyping primers are provided in Supplementary Table 1.

Feulgen analysis

5μm sections of placentas/livers were treated with 1N hydrochloric acid and stained with Schiff reagent. Cytoplasm was counterstained with aqueous light green (1%). Nuclear intensity was quantified using ImageJ (http://rsbweb.nih.gov/ij/)[48]. TGC ploidy was expressed relative to 2C-4C labrynthine trophoblast cells. For binucleated TGCs, ploidy levels of individual nuclei were summed to derive cumulative ploidy. Hepatocyte ploidy was expressed relative to 2C–4C hepatocytes deficient for *E2f7/EfF8*. Hepatocyte ploidy was expressed on a per nucleus basis.

Flow cytometry analysis

Nuclei suspensions were obtained from frozen liver tissue as previously described[49]. Total DNA content of minimum 30,000 nuclei per liver sample were analyzed using LSR II (BD Biosciences). Cell cycle profiles were generated using FlowJo (Tree Star).

Affymetrix analyses

Total RNA was extracted from minimum 3 livers per genetic group using TRIzol (Invitrogen). RNA quality was verified using Agilent 2100 Bioanalyzer, and samples submitted to OSUCCC Microarray Shared Resource facility for biotinylated cRNA generation and MOE4302.0 hybridization. GeneChip Scanner 3000 (Affymetrix) was used for data acquisition. Pre-processing of raw signal intensities was performed using the Robust Multi-chip Average (RMA) method[50]. BRB-Array Tools 3.8.1 was then used to identify differentially expressed genes[51]. For heatmap images, geometric mean of genes after RMA normalization from control liver samples was set as reference, with colors corresponding to the ratio between expression of genes in mutant samples and the reference. Functional annotation was performed using Ingenuity Pathway Analysis (Ingenuity Systems).

NanoString analyses

From each tissue sample, total RNA (200ng) was profiled on a custom codeset containing 200 selected genes following manufacturer's instructions (Supplementary Table 3). For TGC gene expression analysis, we isolated TGCs from frozen placenta sections using laser capture microdissection (PALM MicroLaser system). Total RNA was then extracted using Arcturus PicoPure RNA Isolation Kit (Applied Biosystems 12204-01). For validation of gene expression changes in the liver (Supplementary Fig. 4a), the same set of TRIzol-isolated RNA was utilized in both Affymetrix and NanoString assays. The NanoString data is first normalized to the geometric mean of positive control spike counts in each lane of the cartridge, followed by subtracting the minimum negative control spike counts in each lane to remove the background. Finally, expression of each gene in the codeset is normalized with respect to the geometric mean of the housekeeping genes. Heatmaps were generated in the same manner as for Affymetrix gene expression data.

Confocal microscopy-3D reconstruction

70μm section of tissues were stained with 1mM Draq5 (Biostatus) at 4°C overnight. Sections were examined by confocal laser scanning microscopy (Zeiss LSM 510) at 63X and 0.7X scan zoom. Optical sections with between-plane-plane resolution of 0.40μm and axial resolution of 0.42μm were acquired. 4 to 5 non-overlapping regions per placenta were imaged with a field view of 207μm × 207μm and depth of 40 ± 2μm, resulting in a stack of 100 images for each region. This process was identically repeated for liver samples. For 3D reconstruction, the image stacks were processed using Insight Toolkit and ITK-SNAP[52]. Each nucleus was segmented by active contour segmentation using region competition as the stopping criterion[53]. Nuclei of binucleated TGCs were constructed separately and assigned different colors. Only the volumes of individual hepatocyte nuclei were measured.

Transmission Electron Microscopy

Placentas were fixed/processed following a standard protocol (http://cmif.osu.edu/419.cfm) and embedded in Eponate resin. 70nm placental cross sections were mounted on copper grids, double stained with uranyl acetate and lead citrate, and observed with a Technai G2 Spirit transmission electron microscope (FEI).

Transient transfections

For HepG2, subconfluent cells were transfected with 1:3 ratio of plasmid DNA:reagent [X-tremeGENE HP DNA Transfection Reagent (Roche)] in 10% FBS RPMI-1640. Cells were collected 48 hours after transfection. In 1 experiment, 3 100cm plates of transfected cells were combined for lysis and sonication as 1 sample in the chromatin immunoprecipitation (ChIP) assay. For Rcho-1, transfection conditions were same as described for HepG2 cells. Rcho-1 cells were maintained as previously described[54]. In 1 experiment, two 150cm plates were combined as one sample utilized in the ChIP. A total of 3 independent experiments for each cell line was performed. For HEK293 cells, subconfluent cells in 10% FBS DMEM were transfected using calcium phosphate with 25μg of plasmid DNA expressing wildtype flag-E2F7/flag-E2F8 or mutant flag-E2F7/flag-E2F8.

Systemic administration of plasmid DNA

Six-week-old wildtype male mice were injected with either sterile PBS or sterile PBS containing 10μg plasmid DNA through the tail vein following a published protocol[55]. Mice were sacrificed by CO_2 asphyxiation 24 hours after TV injection. Whole body perfusion with warm saline was performed using the intracardiac method prior to excision of the liver, subsequent derivation of single-celled suspension by passing perfused tissue through 40μm mesh and fixation/processing for chromatin immunoprecipitation assays (next section).

Chromatin immunoprecipitation assays

For HepG2 and Rcho-1 TS cell lines, transfected cells were cross-linked in growth media containing 1% formaldehyde followed by neutralization with 1.25M glycine. The cytoplasmic fraction was discarded (cytoplasmic lysis buffer: 5mM PIPES pH 8.0, 85mM KCl, 0.5% NP40 and fresh protease inhibitors). Nuclear lysates were collected by incubating the nuclei pellet in lysis buffer containing 50mM Tris pH 8.0, 10mM EDTA, 0.3% SDS and fresh cocktail of protease/phosphatase inhibitors. Sonicated chromatin (~100–300bp) was incubated with 10μg of anti-Flag mouse monoclonal antibodies (Sigma F1804) or normal mouse IgG (Santa Cruz sc-2025) at 4°C overnight. Antibody-protein-DNA complexes were recovered by addition of 50% Protein G agarose slurry (Millipore 16–266) pre-cleared with 10mg/ml tRNA and 10mg/ml BSA. De-crosslinking was performed at 65°C overnight with periodic agitation. Recovered DNA was purified using Qiagen PCR extraction kit. 5% input and 2μl of eluted DNA was used for quantitative Real-Time PCR (RT-PCR) with gene-specific primers and SYBR Green (BioRad 170–8880). For HEK293 cells, the EZ-CHIP assay kit (Millipore 17–371) was used following manufacturer's instructions. Sonicated chromatin was incubated with 2μg of anti-Flag antibodies (Sigma F1804) or normal mouse IgG (Santa Cruz sc-2025) at 4°C overnight. Antibody-protein-DNA complexes were recovered by addition of Salmon Sperm DNA/Protein G agarose slurry (Millipore 16–201). Immunoprecipitated DNA fractions were de-crosslinked at 65°C overnight and purified using QIAquick columns (QIAGEN). Quantitative RT-PCR was performed as above except 1% input was used. All quantitative RT-PCRs reactions were performed in triplicate using the following conditions: 1 cycle at 95°C 5 min, followed by 20–40 cycles of 95°C 15 sec, 60–64°C 30 sec and 72°C 30 sec.

Immunoblot assays

Whole cell lysates were prepared from lysis of HepG2 and Rcho-1 TS cells in a standard radioimmunoprecipitation (RIPA) buffer containing freshly diluted cocktail of protease and phosphatase inhibitors. For preparation of liver lysates, frozen tissue (~100mg) was thawed on ice followed by homogenization in RIPA buffer and then centrifugation at maximum speed for 15 minutes in 4°C. Total protein concentration was measured using the Bio-Rad Protein Assay kit (BioRad 500-0006). Denatured samples were separated in 8–10% SDS-polyacrylamide gels, transferred onto PDVF membranes, blocked in 5% milk-PBS solution and incubated overnight in 4°C with the following primary antibodies: anti-E2F3 1:5000 (Santa Cruz sc-878x), anti-Flag 1:1000 (Sigma F1804), anti-Tubulin 1:5000 (Sigma T6199) and anti-HSP70 1:5000 (BD Transduction Laboratories 610608). HRP-conjugated species-

specific secondary antibodies were applied to membranes followed by detection with SuperSignal West Femto kit (Thermo Scientific 34095).

Immunohistochemistry and immunofluoresence

After antigen retrieval using Target Retrieval Solution (DAKO S1699), 5μm deparaffinized sections of placenta or liver tissues were incubated with primary antibodies at 4°C overnight against E2F7 1:100 (Abcam ab56022), E2F8 1:50 (polyclonal against residues 576–595 of murine E2F8), BrdU 1:100 (DAKO MO-0744), Ki67 1:100 (BD Pharmingen 550609), phospho-Histone 3 (Ser10) 1:100 (Millipore 06-570), Cyclin A2 1:100 (Santa Cruz sc-596), Cyclin B1 1:100 (Santa Cruz sc-752), E-Cadherin 1:100 (Abcam ab53033), p57Kip2 1:100 (Santa Cruz sc-8298)[56, 57] and placental lactogen 1:200 (PL-1, F. Talamantes). TGCs in M phase (Fig. 2h) were identified by detecting P-H3 or the lineage-specific PL-1 protein. For IF detection, fluorophore-conjugated secondary antibodies were applied to the slides. For IHC, the VECTASTAIN ABC system was utilized (Vector Laboratories).

BrdU incorporation assays

Pregnant females (E10.5) received a single intraperitoneal injection of bromodeoxyuridine (BrdU, Sigma B5002) in sterile PBS at 100μg/g body weight 1 hour prior to sacrifice for collection of placentas. 5μm deparaffinized tissue sections were used for BrdU detection after incubation in 2N HCl and neutralization with 10mM sodium borate (pH 8.0). Primary antibody was then applied overnight.

pIpC injections

6-week-old mice received 5 intraperitoneal injections of 250μg of polyinosine-polycytidine (pIpC, Sigma P1530) dissolved in sterile PBS every alternate day. Mice were sacrificed 24 hours after the last injection, and their livers harvested for flow cytometry and microarray analyses.

Carbon tetrachloride injection

6-month-old mice received a single intraperitoneal injection of 10% carbon tetrachloride (Sigma 319961) dissolved in corn oil. Mice were sacrificed at 0, 24, 48, 60 and 168 hours (when liver regeneration is complete in rodents[58]) post-injection. Mice were administered an intraperitoneal injection of BrdU solution (100μg/g body weight) to label hepatocytes in S phase of the cell cycle 1 hour prior to sacrifice.

Tamoxifen induction of *cre*

Tamoxifen chow (Teklad Lab Animal Diets, Harlan Laboratories) was prepared by mixing 3kg of irradiated standard chow with 1g tamoxifen (Sigma T5648). For pre-weaning induction of *cre*, 7-day-old pups and their mother were switched from regular to tamoxifen chow for 1 week. After 1 week, they were again fed regular chow until weaning and up to time of sacrifice (age 2 months). For post-weaning induction of *cre*, pups were weaned from their mother at age 21 days and maintained on tamoxifen chow starting from age 28 days up to age 2 months. Tamoxifen chow was stored in the dark at 4°C and changed weekly. It was provided to mice at 40–80mg/kg body weight[59].

X-gal staining

OCT-embedded placentas were sectioned and fixed in 0.2% PBS-glutaraldehyde solution (1.25mM EGTA pH 7.3 and 2mM $MgCl_2$). Sections were rinsed with wash buffer [2mM $MgCl_2$, 0.01% sodium deoxycholate and 0.02% IGEPAL CA-630 (Sigma I8896)] and stained in LacZ solution (4mM potassium ferricyanide, 4mM potassium ferrocyanide and 1mg/ml X-gal in wash buffer) at 37°C overnight with protection from light. Nuclear Fast Red was used as counterstain.

E2F Binding site analysis

Promoter sequences (−3000bp ~ +2000bp) of genes antagonistically regulated by E2F1-3 and E2F7/E2F8 were obtained from the UCSC genome browser (http://genome.ucsc.edu/). E2F consensus binding sites were identified using TFSearch (http://www.cbrc.jp/research/db/TFSEARCH.html).

Statistical analyses

Binucleated TGCs, as a percentage of minimum 143 total TGCs assessed in each genetic group, was quantified in confocal images using the LSM image browser (Zeiss). All other IHC/IF-associated quantification of TGCs/hepatocytes was performed using Metamorph 6.1 in photomerged images (placenta) or 5–7 random images (liver) acquired at 40× from minimum of 3 sections per sample. Results were reported as an average percentage ± S.D. of positive cells in number (*n*) of control and mutant samples analyzed. Flow cytometry profiles (e.g. Fig. 3f) are representative of minimum 3 independent experiments per genotype and age group. Flow cytometry results were reported as an average percentage ± S.D. of nuclei with certain DNA content out of minimum 30,000 nuclei gated per sample in *n* of control and mutant samples analyzed. Pairwise comparisons were evaluated by 2-tailed Student's T-test, while multiple comparisons were evaluated by One-way ANOVA. When appropriate, p-values were adjusted by the Holm's method within each ploidy category.

Supplementary Material

Refer to Web version on PubMed Central for supplementary material.

ACKNOWLEDGEMENTS

We thank L. Rawahneh, J. Moffitt and N. Lovett for excellent technical assistance with histology, and P. Wenzel for generating and harvesting *123tko* placentas. We also thank these individuals from OSUCCC Shared Resources: T. Wise, J. Palatini, H. Alders, P. Yan, P. Fada and B. Rodriguez (Microarray and Nucleic Acid Shared Resources); B. McElwain (Analytic Cytometry); R. Burry, K. Wolken, and B. Kemmenoe (Microscopy and Imaging); and K. La Perle (Comparative Pathology and Mouse Phenotyping). We are gracious for PL-1 antibodies provided by F. Talamantes, Rcho-1 TS cells from M. Soares and HepG2 cells from S. Jacobs. This work was funded by NIH grants to G.L. (R01CA85619, R01CA82259, R01HD047470, P01CA097189) and P.S. (R01CA132740). G.L. is the recipient of The Pew Charitable Trust Scholar Award and the Leukemia & Lymphoma Society Scholar Award. H.-Z. Chen, M. Mair, S. Senepati, S. Raman and T. Pécot are recipients of the Pelotonia Fellowship Award.

REFERENCES

1. Lilly MA, Duronio RJ. New insights into cell cycle control from the Drosophila endocycle. Oncogene. 2005; 24:2765–2775. [PubMed: 15838513]

2. Varmuza S, Prideaux V, Kothary R, Rossant J. Polytene chromosomes in mouse trophoblast giant cells. Development. 1988; 102:127–134. [PubMed: 3166422]
3. Cross J. How to make a placenta: mechanisms of trophoblast cell differentiation in mice – a review. Placenta. 2005; 26:S3–S9. [PubMed: 15837063]
4. Mehrotra S, Maqbool SB, Kolpakas A, Murnen K, Calvi BR. Endocycling cells do not apoptose in response to DNA rereplication genotoxic stress. Genes Dev. 2008; 22:3158–3171. [PubMed: 19056894]
5. Lee HO, Davidson JM, Duronio RJ. Endoreplication: polyploidy with purpose. Genes Dev. 2009; 23:2461–2477. [PubMed: 19884253]
6. Storchova Z, Pellman D. From polyploidy to aneuploidy, genome instability and cancer. Nature Rev. Mol. Cell. Biol. 2004; 5:45–54. [PubMed: 14708009]
7. Harbour JW, Dean DC. The Rb/E2F pathway: expanding roles and emerging paradigms. Genes Dev. 2000; 14:2393–2409. [PubMed: 11018009]
8. Yamasaki L, et al. Tumor induction and tissue atrophy in mice lacking E2F-1. Cell. 1996; 85:537–548. [PubMed: 8653789]
9. Field SJ, et al. E2F-1 functions in mice to promote apoptosis and suppress proliferation. Cell. 1996; 85:549–561. [PubMed: 8653790]
10. Humbert PO, et al. E2f3 is critical for normal cellular proliferation. Genes Dev. 2000; 14:690–703. [PubMed: 10733529]
11. Murga M, et al. Mutation of E2F2 in mice causes enhanced T lymphocyte proliferation, leading to the development of autoimmunity. Immunity. 2001; 15:959–970. [PubMed: 11754817]
12. Humbert PO, et al. E2F4 is essential for normal erythrocyte maturation and neonatal viability. Mol. Cell. 2000; 6:281–91. [PubMed: 10983976]
13. Rempel RE, et al. Loss of E2F4 activity leads to abnormal development of multiple cellular lineages. Mol. Cell. 2000; 6:293–306. [PubMed: 10983977]
14. Lindeman GJ, et al. A specific, nonproliferative role for E2F-5 in choroid plexus function revealed by gene targeting. Genes Dev. 1998; 12:1092–1098. [PubMed: 9553039]
15. Pohlers M, et al. A role for E2F6 in the restriction of male-germ-cell-specific gene expression. Curr. Biol. 2005; 15:1051–1057. [PubMed: 15936277]
16. Li J, et al. Synergistic function of E2F7 and E2F8 is essential for cell survival and embryonic development. Dev. Cell. 2008; 14:62–75. [PubMed: 18194653]
17. Chen H-Z, Tsai S-Y, Leone G. Emerging roles of E2Fs in cancer: an exit from cell cycle control. Nature Rev. Cancer. 2009; 9:785–797. [PubMed: 19851314]
18. Trimarchi JM, Lees JA. Sibling rivalry in the E2F family. Nature Rev. Mol. Cell Biol. 2002; 3:11–20. [PubMed: 11823794]
19. Lammens T, Li J, Leone G, De Veylder L. Atypical E2Fs: new players in the E2F transcription factor family. Trends Cell Biol. 2009; 19:111–118. [PubMed: 19201609]
20. Breuer C, Ishida T, Sugimoto K. Developmental control of endocycles and cell growth in plants. Curr. Opin. Plant Biol. 2010; 13:654–660. [PubMed: 21094078]
21. Zielke N, et al. Control of Drosophila endocycles by E2F and CRL4(CDT2). Nature. 2011; 480:123–127. [PubMed: 22037307]
22. Barbason H, Van Cantfort J, Houbrechts N. Correlation between tissular and division functions in the liver of young rats. Cell Tissue Kinet. 1974; 7:319–326. [PubMed: 4844544]
23. Dallman PR, Spirito RA, Siimes MA. Diurnal patterns of DNA synthesis in the rat: modification by diet and feeding schedule. J. Nutr. 1974; 104:1234–1241. [PubMed: 4472065]
24. Tsai S-Y, et al. Mouse development with a single E2F activator. Nature. 2008; 454:1137–1141. [PubMed: 18594513]
25. Chong J-L, et al. E2f1-3 switch from activators in progenitor cells to repressors in differentiating cells. Nature. 2009; 462:930–934. [PubMed: 20016602]
26. Wenzel P, et al. Cell proliferation in the absence of E2F1-3. Dev. Biol. 2010; 351:35–45. [PubMed: 21185283]
27. Kuhn R, Schwenk F, Aguet M, Rajewsky K. Inducible gene targeting in mice. Science. 1995; 8:1427–1429. [PubMed: 7660125]

28. de Bruin A, et al. Identification and characterization of E2F7, a novel mammalian E2F family member capable of blocking cellular proliferation. J. Biol. Chem. 2003; 278:42041–42049. [PubMed: 12893818]
29. Di Stefano L, et al. E2F7, a novel E2F featuring DP-independent repression of a subset of E2F-regulated genes. EMBO J. 2003; 22:6289–6298. [PubMed: 14633988]
30. Maiti B, et al. Cloning and characterization of mouse E2F8, a novel mammalian E2F family member capable of blocking cellular proliferation. J. Biol. Chem. 2005; 280:18211–18220. [PubMed: 15722552]
31. Christensen J, et al. Characterization of E2F8, a novel E2F-like cell-cycle regulated repressor of E2F-activated transcription. Nucleic Acids Res. 2005; 33:5458–5470. [PubMed: 16179649]
32. Ouseph MM, et al. Atypical E2F repressors and activators coordinate placental development. Dev. Cell. 2012; 22:849–862. [PubMed: 22516201]
33. Postic C, Magnuson MA. DNA excision in liver by an albumin-cre transgene occurs progressively with age. Genesis. 2000; 26:149–150. [PubMed: 10686614]
34. Margall-Ducos G, Celton-Morizur S, Couton D, Bregerie O, Desdouets C. Liver tetraploidization is controlled by a new process of incomplete cytokinesis. J. Cell Sci. 2007; 120:3633–3639. [PubMed: 17895361]
35. Schuler M, Dierich A, Chambon P, Metzger D. Efficient temporally controlled targeted somatic mutagenesis in hepatocytes of the mouse. Genesis. 2004; 39:167–172. [PubMed: 15282742]
36. Normand G, King RW. Understanding cytokinesis failure. Adv. Exp. Med. Biol. 2010; 676:27–55. [PubMed: 20687468]
37. Ullah Z, Lee CY, Lilly MA, DePamphilis ML. Developmentally programmed endoreduplication in animals. Cell Cycle. 2009; 8:1501–1509. [PubMed: 19372757]
38. Sorensen CS, et al. A conserved cyclin-binding domain determines functional interplay between anaphase-promoting complex-Cdh1 and cyclin A-Cdk2 during cell cycle progression. Mol. Cell. Biol. 2001; 21:3692–3703. [PubMed: 11340163]
39. Kalaszczynska I, et al. Cyclin A is redundant in fibroblasts but essential in hematopoietic and embryonic stem cells. Cell. 2009; 138:352–365. [PubMed: 19592082]
40. Edgar BA, Orr-Weaver TL. Endoreplication cell cycles: more for less. Cell. 2001; 105:297–306. [PubMed: 11348589]
41. Inzé D, De Veylder L. Cell cycle regulation in plant development. Annu. Rev. Genet. 2006; 40:77–105. [PubMed: 17094738]
42. Duronio RJ, O'Farrell PH, Xie JE, Brook A, Dyson N. The transcription factor E2F is required for S phase during Drosophila embryogenesis. Genes Dev. 1995; 9:1445–1455. [PubMed: 7601349]
43. Weng L, Zhu C, Xu J, Du W. Critical role of active repression by E2F and Rb proteins in endoreplication during Drosophila development. EMBO J. 2003; 22:3865–3875. [PubMed: 12881421]
44. Lammens T, et al. Atypical E2F activity restrains APC/CCCS52A2 function obligatory for endocycle onset. Proc. Natl. Acac. Sci U.S.A. 2008; 105:14721–14726.
45. Kohn MJ, Bronson RT, Harlow E, Dyson NJ, Yamasaki L. Dp1 is required for extra-embryonic development. Development. 2003; 130:1295–1305. [PubMed: 12588846]
46. Krek W, et al. Negative regulation of the growth-promoting transcription factor E2F-1 by a stably bound cyclin A-dependent protein kinase. Cell. 1994; 78:161–172. [PubMed: 8033208]
47. Krek W, et al. Cyclin A-kinase regulation of E2F-1 DNA binding function underlies suppression of an S phase checkpoint. Cell. 1995; 83:1149–1158. [PubMed: 8548802]
48. Hardie DC, Gregory TR, Hebert PD. From pixels to picograms: a beginners' guide to genome quantification by Feulgen image analysis densitometry. J. Histochem. Cytochem. 2002; 50:735–749. [PubMed: 12019291]
49. Mayhew CN, et al. Liver-specific pRB loss results in ectopic cell cycle entry and aberrant ploidy. Cancer Res. 2005; 65:4568–4577. [PubMed: 15930274]
50. Irizarry RA, et al. Summaries of Affymetrix GeneChip probe level data. Nucleic Acids Res. 2003; 31:e15. [PubMed: 12582260]

51. Bolstad BM, Irizarry RA, Astrand M, Speed TP. A Comparison of normalization methods for high density oligonucleotide array data based on bias and variance. Bioinformatics. 2003; 19:185–193. [PubMed: 12538238]

52. Yushkevich PA, et al. User-guided 3D active contour segmentation of anatomical structures: significantly improved efficiency and reliability. NeuroImage. 2006; 31:1116–1128. [PubMed: 16545965]

53. Zhu SC, Yuille A. Region competition: unifying snakes, region growing, and bayes/mdl for multiband image segmentation. IEEE Trans. Pattern Anal. 1996; 18:884–900.

54. Sahgal N, Canham LN, Canham B, Soares MJ. Rcho-1 trophoblast stem cells: a model system for studying trophoblast cell differentiation. Methods Mol. Med. 2006; 121:159–178. [PubMed: 16251742]

55. Liu F, Song YK, Liu D. Hydrodynamic-based transfection in animal by systemic administration of plasmid DNA. Gene Therapy. 1999; 6:1258–1266. [PubMed: 10455434]

56. Ullah Z, Kohn MJ, Yagi R, Vassilev LT, DePamphilis ML. Differentiation of trophoblast stem cells into giant cells is triggered by p57/Kip2 inhibition of CDK1 activity. Genes Dev. 2008; 22:3204–3236.

57. Nagahama H, et al. Spatial and temporal expression patterns of the cyclin-dependent kinase (CDK) inhibitors p27Kip1 and p57Kip2 during mouse development. Anat. Embryol. 2001; 203:77–87. [PubMed: 11218061]

58. Schultze, B.; Gerhard, H.; Maurer, W. Liver Regeneration after Experimental Injury. New York: Grune and Stratton; 1975. A quantitative model of liver regeneration in the mouse after CCl4 intoxification.

59. Kiermayer C, Conrad M, Schneider M, Schmidt J, Brielmeier M. Optimization of spatiotemporal gene inactivation in mouse heart by oral application of tamoxifen citrate. Genesis. 2007; 45:11–16. [PubMed: 17216603]

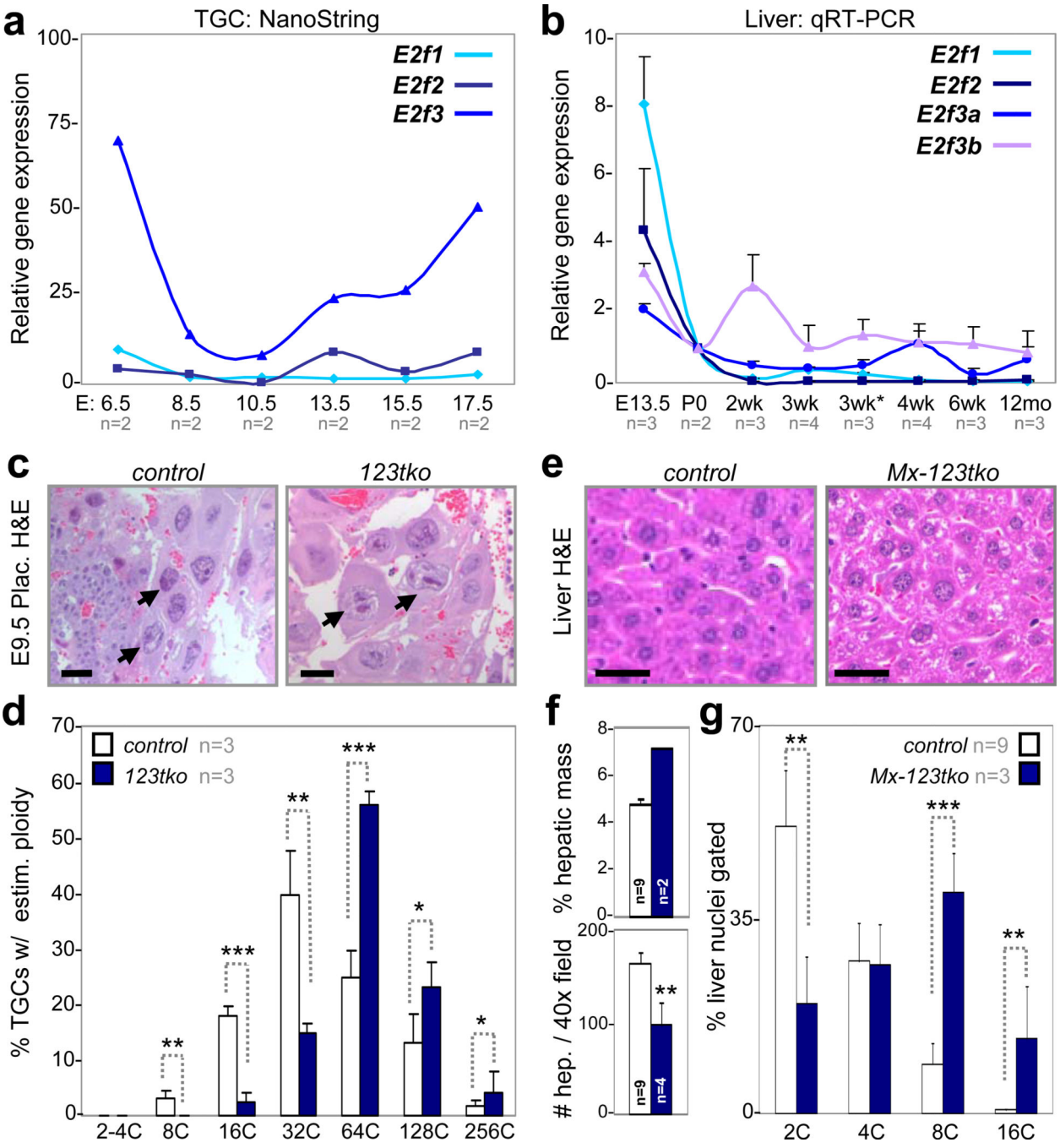

Figure 1. Loss of *E2f* activators promotes TGC and hepatocyte endocycles

a, NanoString analysis of TGC-specific *E2f1-3* expression in laser capture microdissected wild type cells, n=2 placentas analyzed per time point. **b**, Quantitative RT-PCR analysis of *E2f* activators in pre- (E13.5) and post-natal (P0-12mo) wild type livers, with n per time point as indicated. 3wk*, 1 day post weaning (3wk). **c,** Representative E9.5 H&E placenta sections showing *control* and *E2f1*$^{-/-}$;*E2f2*$^{-/-}$;*E2f3*$^{-/-}$ (*123tko*) TGCs. Arrows point to selected TGCs. Scale bar, 12.5μm. **d,** Feulgen quantification of ploidy in E9.5 *control* and *123tko* TGCs, n=3 per genetic group. One-way ANOVA, * p≤0.05, ** p≤0.01, *** p≤0.001.

e, Representative H&E sections showing *control* and *Mx-cre;E2f1*$^{-/-}$*;E2f2*$^{-/-}$*;E2f3*$^{f/f}$ (*Mx-123tko*) livers of 8-week-old mice 10 days after pIpC injection. Scale bar, 10μm. **f,** Measurements showing enlarged *Mx-123tko* livers (top graph) and hepatocytes (bottom graph) relative to *control* tissues and hepatocytes, with n per genetic group as indicated. Two-tailed Student T-test, ** p≤0.01. **g,** Flow cytometry of *control* and *Mx-123tko* liver nuclei from 8-week-old mice, with n per genetic group as indicated. One-way ANOVA, ** p≤0.01, *** p≤0.001. **c** *control*, wild type TGCs; **e** *control*, pIpC injected *Mx-cre;E2f1*$^{-/-}$*;E2f2*$^{-/-}$*;E2f3*$^{+/+}$ livers; **f-g** *control*, wild type livers. Data in **a**, **b**, **d**, **f** and **g** reported as average values, ± SD are included when n>2 samples were analyzed.

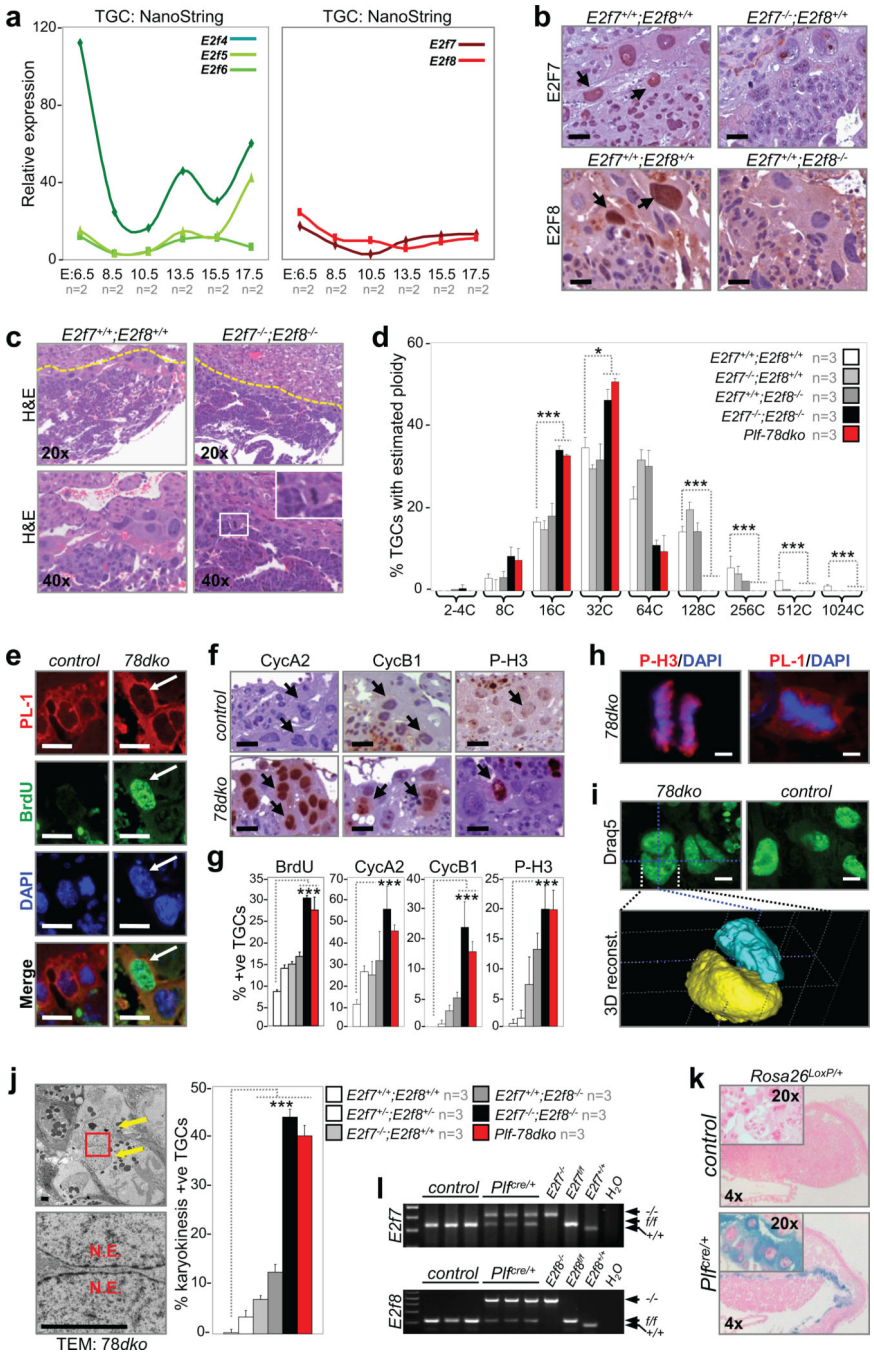

Figure 2. *E2f7* and *E2f8* promote TGC endocycles

a, NanoString analysis of TGC-specific *E2f4-6* (left panel) and *E2f7/E2f8* (right panel) expression in laser capture microdissected wild type cells, n=2 placentas analyzed per time point. **b,** Immunohistochemistry demonstrating E2F7 (top left) and E2F8 (bottom left) expression in wild type E10.5 TGCs but not mutant controls. Arrows point to selected TGCs. Scale bar, 10μm. **c,** Representative H&E sections of E10.5 *control* and *E2f7*$^{-/-}$;*E2f8*$^{-/-}$ (*78dko*) placentas. Inset, a *78dko* TGC in metaphase. **d,** Feulgen quantification of genome ploidy in E10.5 TGCs, n=3 placentas analyzed per genetic group.

e–g, Immunostaining and quantification of S and M phase proteins in E10.5 *control* and *78dko* TGCs. Arrows point to TGCs. n=3 placentas analyzed per genetic group. Scale bar in **e–f**, 12.5μm. **h,** Co-immunofluorescence showing E10.5 *78dko* TGCs in anaphase (left, P-H3) and metaphase (right, PL-1). DAPI stained total DNA. Scale bar, 5μm. **i,** Representative confocal images of nuclei in E10.5 *control* and *78dko* TGCs (top) and 3D reconstruction of a binucleated *78dko* TGC (bottom). Draq5 stained total DNA pseudocolored in green. Scale bar, 10μm. **j,** Left, transmission electron micrograph of a *78dko* E10.5 TGC (left top, arrows indicate two nuclei; left bottom, enlarged view of boxed area showing separation between nuclear envelopes). Right, quantification of binucleated E10.5 TGCs, n=3 placentas analyzed per genetic group. **k,** X-gal staining of E10.5 *control* and $Plf^{cre/+}$ placentas carrying the reporter allele $Rosa26^{LoxP}$. **l,** PCR genotyping of genomic DNA isolated from laser capture microdissected E10.5 *control* and $Plf^{cre/+}$ TGCs. **e**, **f** and **i** *control*, $E2f7^{+/+};E2f8^{+/+}$; **e**, **f** and **h**–**j** *78dko*, $E2f7^{-/-};E2f8^{-/-}$; **k** *control*, $Plf^{+/+};Rosa26^{LoxP/+}$; **l** *control*, $Plf^{+/+};E2f7^{f/f};E2f8^{f/f}$; **d**, **g**, and **j** *Plf-78dko*, $Plf^{cre/+};E2f7^{f/f};E2f8^{f/f}$. PL-1, placental lactogen 1; N.E., nuclear envelope. Data in **a**, **d**, **g** and **j** reported as average values, ± SD are included when n>2 samples were analyzed. One-way ANOVA, * $p \leq 0.05$; ** $p \leq 0.01$; *** $p \leq 0.001$.

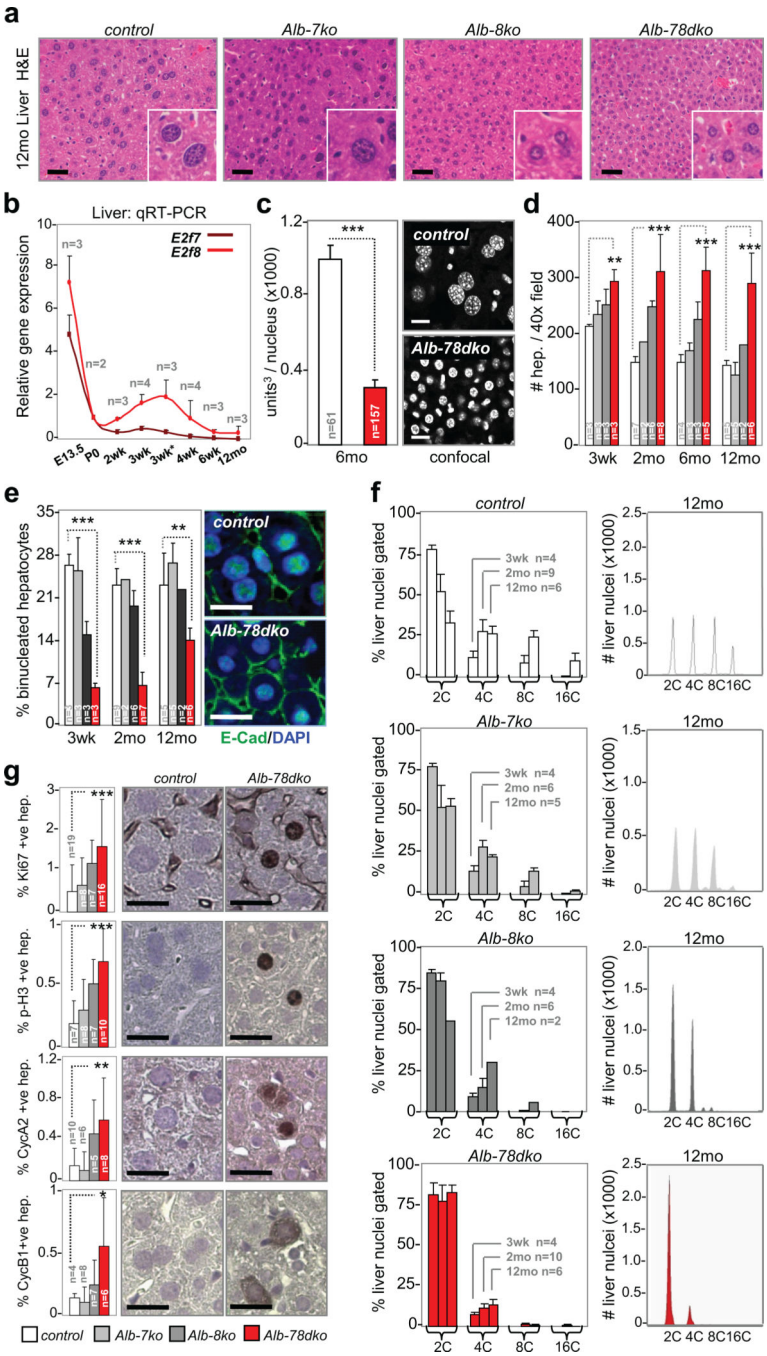

Figure 3. *E2f8* is sufficient to promote hepatocyte endocycles

a, Representative H&E sections of aged (12mo) livers. Scale bar, 12.5μm. **b,** Quantitative RT-PCR analysis of *E2f7* and *E2f8* in pre- (E13.5) and post-natal (P0-12mo) wild type livers, with n per time point analyzed as indicated. 3wk*, 1 day post weaning (3wk). **c,** Left graph, assessment of nuclei volume by confocal imaging and 3-D reconstruction in 6-month-old *control* and *Alb-78dko* hepatocytes. n, number of nuclei evaluated per genotype. Right panels, representative confocal images of DAPI-stained liver sections. Scale bar, 10μm. **d,** Assessment of hepatocyte size in young (3wk), adult (2-6mo) and aged (12mo) livers by

quantifying number of hepatocytes per image field, with n per genetic group analyzed as indicated. **e,** Left graph, quantification of binucleated hepatocytes in young, adult and aged livers, with n per genetic group analyzed as indicated. Right panels, immunofluoresence with anti-E-cadherin marking the boundary of mono- or binucleated hepatocytes. Scale bar, 10μm. **f,** Left column, flow cytometry of liver nuclei in young, adult and aged livers. n, number of livers analyzed per genotype and age group. Right column, representative FACS profiles of liver nuclei from aged (12mo) mice. **g,** Immunohistochemistry and quantification of hepatocyte proliferation in 2-month-old livers, with n per genetic group analyzed as indicated. Scale bar, 10μm. *control*, *E2f7*$^{f/f}$;*E2f8*$^{f/f}$; *Alb-7ko*, *Alb-cre;E2f7*$^{f/f}$; *Alb-8ko*, *Alb-cre;E2f8*$^{f/f}$; *Alb-78dko*, *Alb-cre;E2f7*$^{f/f}$;*E2f8*$^{f/f}$. FACS, fluorescence activated cell sorting. Data in **b**–**g** reported as average values, ± SD are included when n>2 samples were analyzed. One-way ANOVA, * p≤0.05; ** p≤0.01; ***p≤0.001.

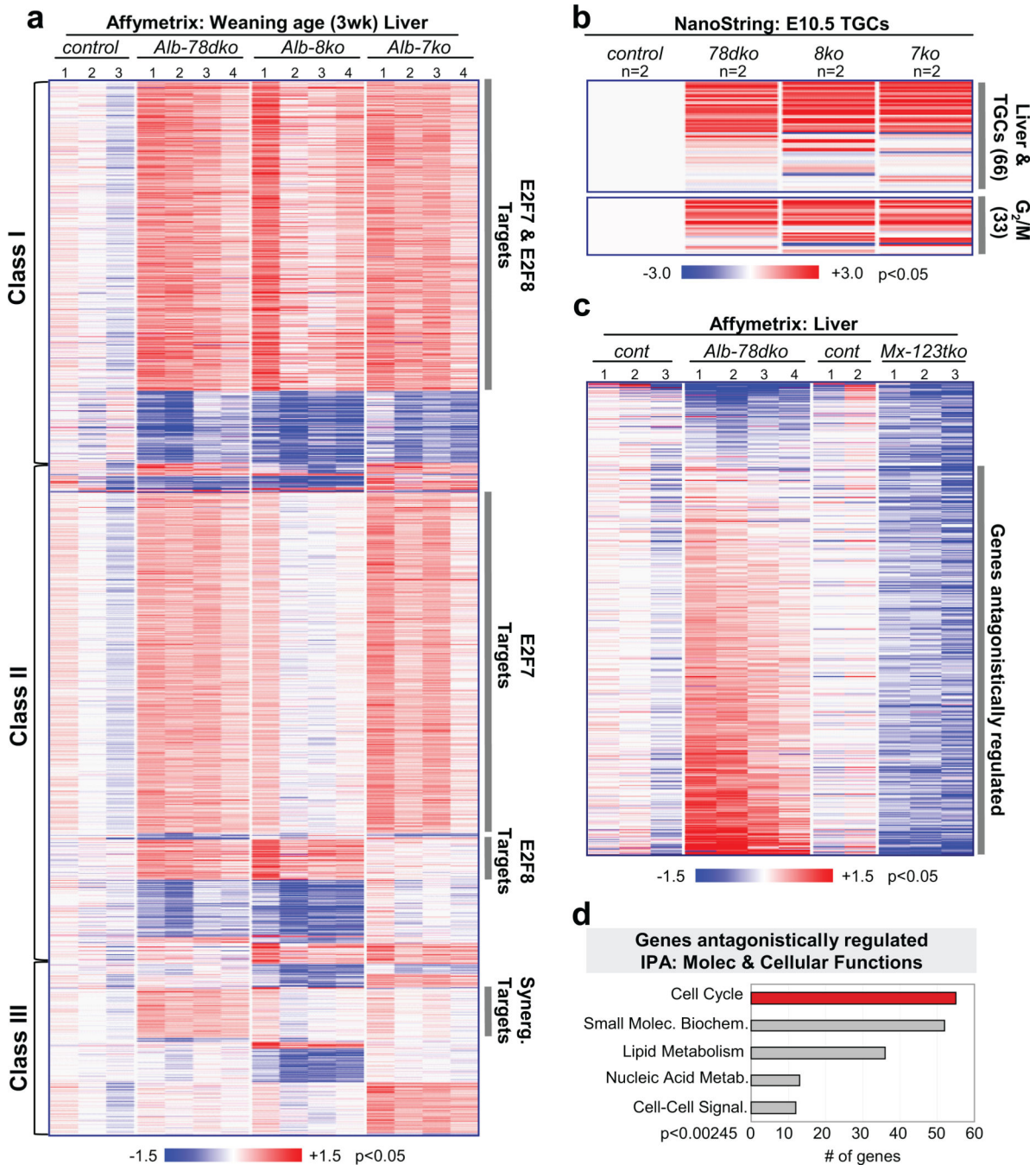

Figure 4. Canonical activator and atypical repressor E2Fs regulate key transcriptional networks coordinating endocycles

a, Heatmap of approximately 4,500 differentially expressed genes in weaning age (3wk) livers. Class I: genes regulated by E2F7 and E2F8. Class II: genes regulated by either E2F7 or E2F8. Class III: genes synergistically regulated by E2F7/E2F8. n=3–4 livers analyzed per genetic group. *control*, *E2f7*$^{f/f}$;*E2f8*$^{f/f}$; *Alb-78dko*, *Alb-cre;E2f7*$^{f/f}$;*E2f8*$^{f/f}$; *Alb-8ko*, *Alb-cre;E2f8*$^{f/f}$; *Alb-7ko*, *Alb-cre;E2f7*$^{f/f}$. **b,** Top, heatmap of TGC gene expression in a custom NanoString mRNA codeset. RNA was isolated from laser capture microdissected E10.5

TGCs in frozen placental tissues. Bottom, G_2/M-related genes in NanoString codeset with deregulated expression in TGCs. n=2 placentas analyzed per genetic group. *control*, *E2f7*$^{+/+}$;*E2f8*$^{+/+}$; *78dko*, *E2f7*$^{-/-}$;*E2f8*$^{-/-}$; *8ko*, *E2f7*$^{+/+}$;*E2f8*$^{-/-}$; *7ko*, *E2f7*$^{-/-}$;*E2f8*$^{+/+}$. **c,** Heatmap of downregulated genes in *Mx-123tko* livers with significantly deregulated expression in *Alb-78dko* livers. n=3–4 livers analyzed per genetic group. *Alb-78dko*, *Alb-cre;E2f7*$^{f/f}$;*E2f8*$^{f/f}$; *Mx-123tko*, *Mx-cre;E2f1*$^{-/-}$;*E2f2*$^{-/-}$;*E2f3*$^{f/f}$. **d,** Top five Molecular & Cellular Functions revealed through Ingenuity Pathway Analysis (IPA) of genes antagonistically regulated by E2F1-3 and E2F7/E2F8.

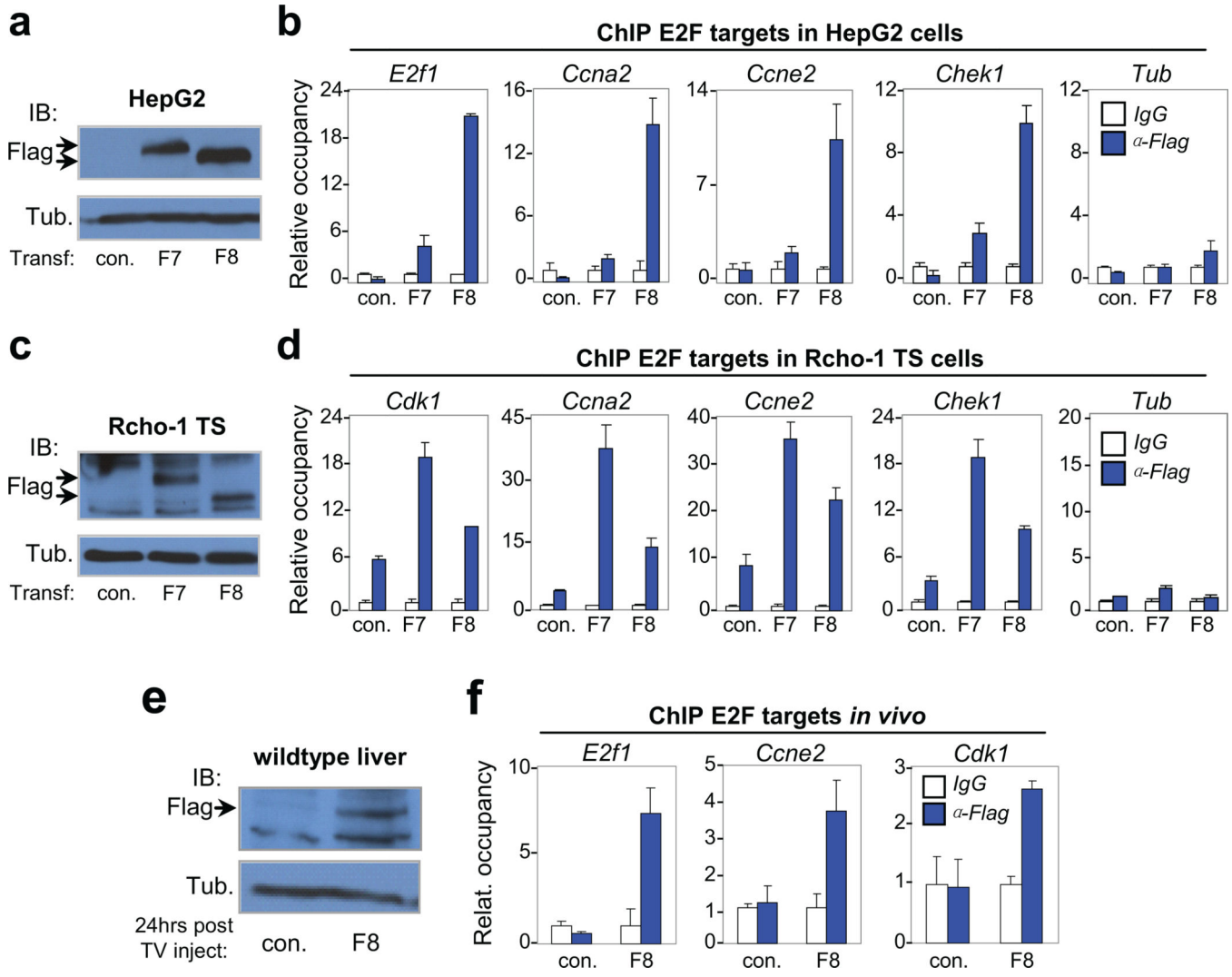

Figure 5. Atypical repressors E2F7/E2F8 directly bind gene targets involved in endocycle control

a, Immunoblot of transfected HepG2 cells showing exogenous expression of flag-tagged E2F7 (F7) and E2F8 (F8) proteins with Tubulin as control. Arrows indicate tagged protein. **b,** Representative chromatin immunoprecipitation (ChIP) assay in transfected HepG2 cells with anti-Flag antibodies demonstrating enhanced occupancy of F7 and F8 proteins on E2F binding sites in the promoter of G_1/S (*E2f1 and Ccne2*) and G_2/M (*Ccna2* and *Chek1*) genes. The *Tubulin* (*Tub*) gene, a non-E2F target, demonstrates specific recruitment of F7/F8 to target promoters containing consensus E2F binding sequences. n=3 independent transfection-ChIP experiments performed. **c,** Immunoblot of transfected Rcho-1 TS cells showing exogenous expression of F7 and F8 proteins with Tubulin as control. Arrows indicate tagged protein. **d,** Representative ChIP assays in transfected Rcho-1 TS cells of G_1/S and G_2/M genes as in HepG2 cells. n=3 independent transfection-ChIP experiments performed. **e,** Immunoblot of liver lysates from 6-week-old mice demonstrating expression of tagged E2F8 protein. A total of 10μg of plasmid DNA was delivered through tail vein injection. Lysates were prepared from livers 24 hours after injection. Tubulin served as loading control. n=3 and n=5 wild type mice were injected with control (empty) plasmid and

plasmid expressing Flag-E2F8, respectively. One out of 5 had detectable expression of F8 as shown by Western blot (Fig. 5e). **f,** ChIP assay in liver lysates with anti-Flag antibodies demonstrating enhanced occupancy of F8 on E2F binding sites in the promoter of G_1/S (*E2f1 and Ccne2*) and G_2/M (*Cdk1*) genes. **a–f** con., empty plasmid; F7, plasmid expressing flag-tagged E2F7; F8, plasmid expressing flag-tagged E2F8. Data in **b, d** and **f** from the representative experiment are reported as average values from triplicate quantitative RT-PCR reactions ± SD.

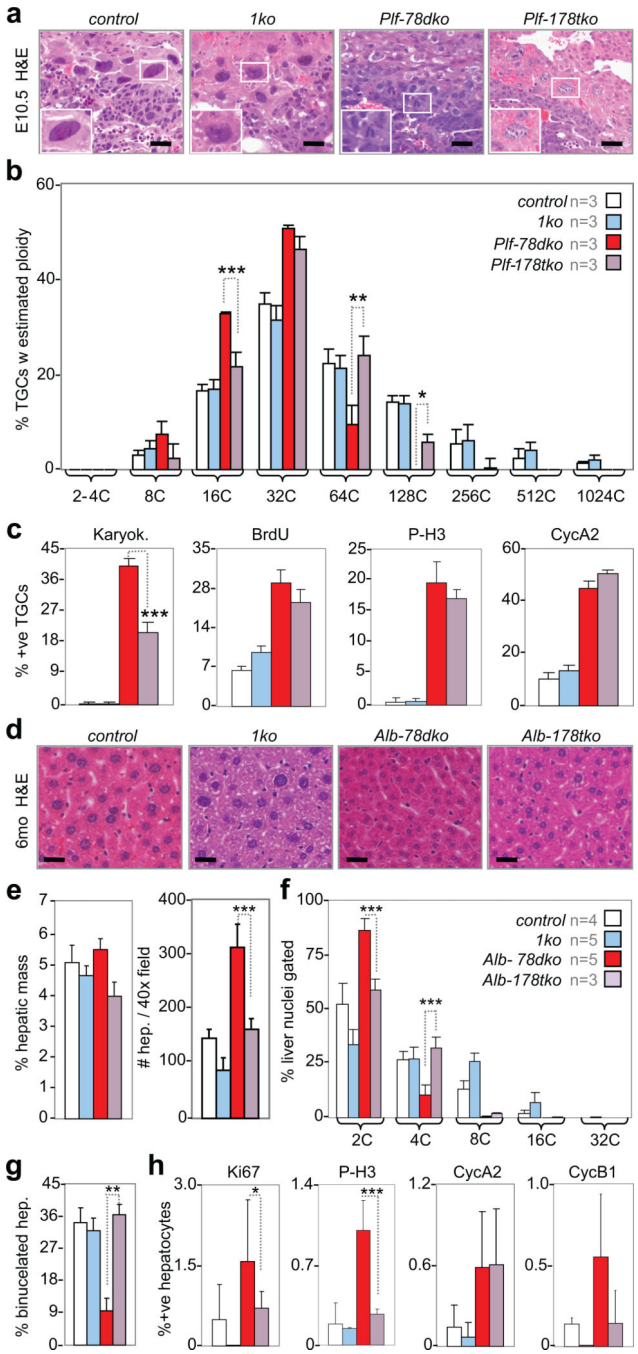

Figure 6. Loss of *E2f1* restores endocycles in *E2f7/E2f8* deficient TGCs and hepatocytes

a, Representative H&E sections of E10.5 TGCs. Scale bar, 12.5μm. **b,** Feulgen quantification of genome ploidy in E10.5 TGCs, n=3 placentas per genetic group analyzed. Note significant increase in proportions of 64C and 128C *Plf-178tko* TGCs relative to *Plf-78dko* TGCs. **c,** Quantification of E10.5 TGCs undergoing karyokinesis and expressing S/M phase markers, n=3 placentas per genetic group analyzed. Note significant reduction in proportion of *Plf-178tko* TGCs undergoing karyokinesis relative to *Plf-78dko* TGCs. **d,** Representative H&E liver sections from 6-month-old mice. Scale bar, 10μm. **e,**

Measurements showing no significant change in percent hepatic mass in 6-month-old mice and a significant decrease in number of hepatocytes per image field in *Alb-178tko* relative to *Alb-78dko* livers, with n per genetic group analyzed as indicated in Fig. 6f. **f,** Flow cytometry of liver nuclei in 6-month-old mice, with n per genetic group analyzed as indicated in legend. Note significant increase and decrease in proportion of 4C and 2C nuclei, respectively, in *Alb-178tko* livers relative to *Alb-78dko* livers. **g,** Quantification of binucleated hepatocytes in 2-month-old livers, with n per genetic group analyzed as indicated in Fig. 6f. **h,** Quantification of hepatocyte proliferation in 2-month-old livers, with n per genetic group analyzed as indicated in Fig. 6f. **a**–**c** *control*, $E2f7^{+/+};E2f8^{+/+}$; **d**-**h** *control*, $E2f7^{f/f};E2f8^{f/f}$; *1ko*, $E2f1^{-/-}$; *Plf-178tko*, $Plf^{cre/+};E2f1^{-/-};E2f7^{f/f};E2f8^{f/f}$; *Alb-178tko*, $Alb\text{-}cre;E2f1^{-/-};E2f7^{f/f};E2f8^{f/f}$. Data in **b**, **c** and **e**-**h** reported as average ± SD. **b** and **f** One-way ANOVA, * p≤0.05; ** p≤0.01; ***p≤0.001. **c**, **e**, **g** and **h**, Two-tailed Student T-test, * p≤0.05; ** p≤0.01; ***p≤0.001.

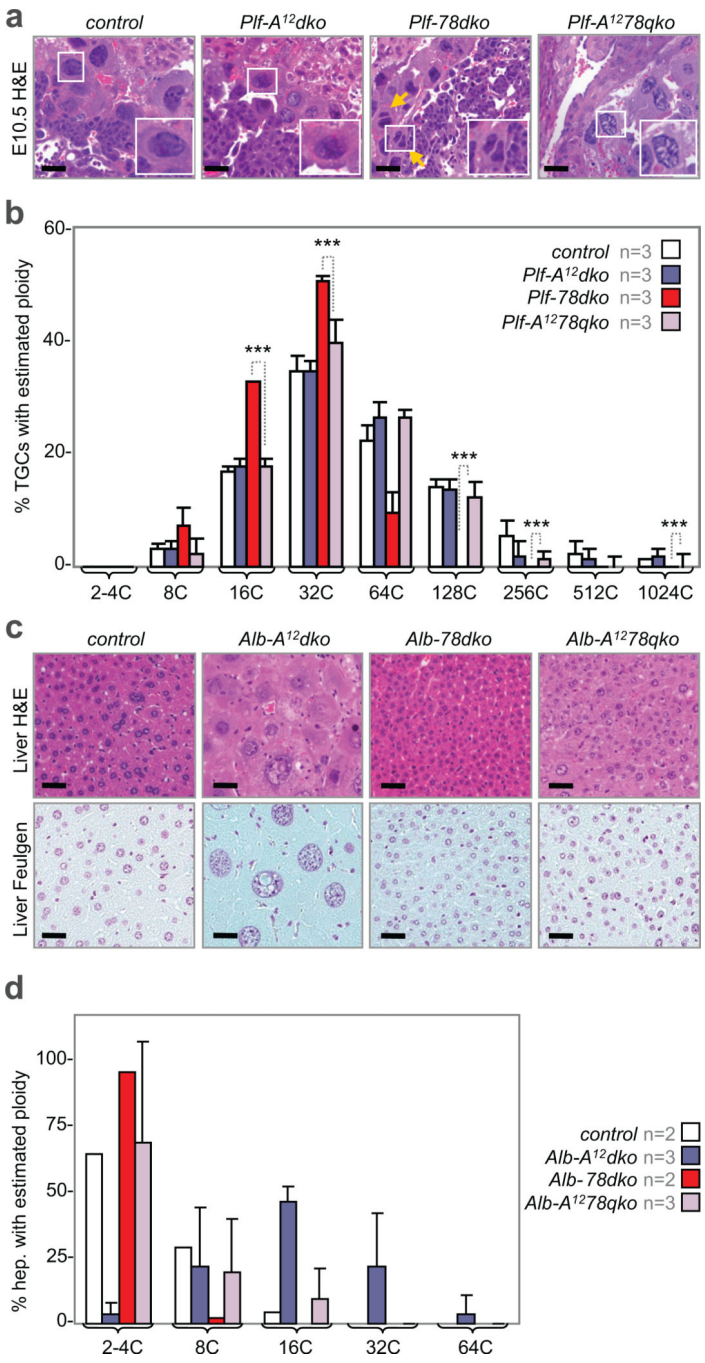

Figure 7. *Cyclin A* ablation reinstates genome ploidy of *E2f7/E2f8* deficient TGCs and hepatocytes

a, H&E images of E10.5 TGCs. The combined loss of *Ccna1* and *Ccna2* (*Plf-A*^{12}*dko*) led to TGCs similar in appearance to *control* TGCs. The additional loss of *Ccna1* and *Ccna2* in *E2f7/E2f8* deficient TGCs (*Plf-A*^{12}*78qko*) led to TGCs with normal (wildtype-like) appearance, in contrast to *Plf-78dko* TGCs that appeared small or were binucleated (yellow arrows). Scale bar, 12.5μm. **b,** Feulgen quantification of genome ploidy in E10.5 TGCs. The intensities (i.e. estimated genome content) of 120–140 TGCs were quantified per placenta

sample, with n placenta samples analyzed per genetic group as indicated. A number of TGCs quadruply deficient for *Ccna1, Ccna2, E2f7* and *E2f8* reach ploidy levels of 128C and 256C. *control*, $E2f7^{f/f};E2f8^{f/f}$; *Plf-A*^{12}, $Plf^{cre/+};Ccna1^{-/-};Ccna2^{f/f}$; *Plf-78dko*, $Plf^{cre/+};E2f7^{f/f};E2f8^{f/f}$; *Plf-A*^{12}*78qko*, $Plf^{cre/+};Ccna1^{-/-};Ccna2^{f/f};E2f7^{f/f};E2f8^{f/f}$. **c,** H&E images of 3-month-old liver sections, which were stained with the Feulgen technique to facilitate quantification of DNA content, showing an increase in both cellular and nuclear size of hepatocytes lacking *Ccna1* and *Ccna2* (*Alb-A*^{12}*dko*) when compared with *control* hepatocytes. Hepatocytes quadruply deficient for *Ccna1*, *Ccna2*, *E2f7* and *E2f8* (*Alb-A*^{12}*78qko*) had nuclei resembling *control* hepatocytes. Scale bar, 12.5μm. **d,** Feulgen quantification of genome ploidy in livers of 3-month-old mice. The intensities (i.e. estimated genome content) of 100 hepatocyte nuclei were quantified per liver sample, with n liver samples analyzed per genetic group as indicated. *Ccna1/Ccna2* deficient livers had increased proportion of hepatocytes with higher ploidy levels (16C, 32C and 64C) relative to *control* livers. Quadruple deficient livers had significantly elevated number of hepatocytes with 16C genomes relative to *Alb-78dko* livers. *control*, $E2f7^{f/f};E2f8^{f/f}$; *Alb-A*^{12}, *Alb-cre*$;Ccna1^{-/-};Ccna2^{f/f}$; *Alb-78dko*, *Alb-cre*$;E2f7^{f/f};E2f8^{f/f}$; *Alb-A*^{12}*78qko*, *Alb-cre*$;Ccna1^{-/-};Ccna2^{f/f};E2f7^{f/f};E2f8^{f/f}$. Data in **b** and **d** reported as average values, ± SD are included when n>2 samples were analyzed. One-way ANOVA, * $p \leq 0.05$; *** $p \leq 0.001$.